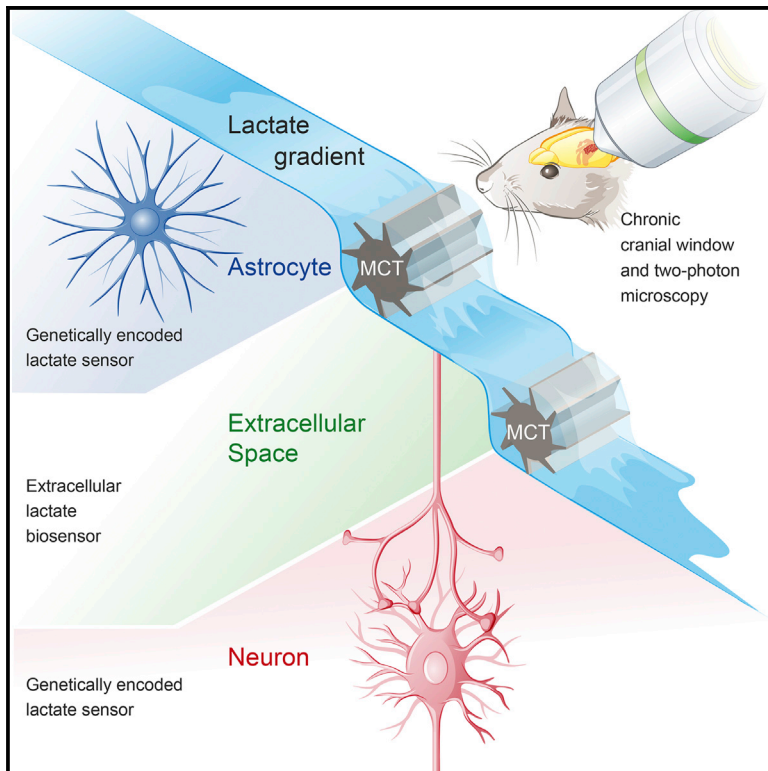# In Vivo Evidence for a Lactate Gradient from Astrocytes to Neurons

Graphical Abstract

Authors

Philipp Mächler, Matthias T. Wyss, Maha Elsayed, ..., Pierre J. Magistretti, L. Felipe Barros, Bruno Weber

Correspondence

bweber@pharma.uzh.ch

In Brief

Mächler et al. used the genetically encoded FRET lactate sensor *Laconic* in combination with in vivo two-photon laser scanning microscopy to monitor lactate dynamics in astrocytes and neurons. Their data support the astrocyte-neuron lactate shuttle model, in which astrocyte-derived lactate acts as an energy substrate for neurons.

Highlights

- Genetically encoded sensor reports intracellular lactate levels in vivo using 2PLSM

- Astrocytes and neurons accumulate intravenously applied L-lactate

- Astrocytes maintain significantly higher lactate levels than neurons

- This lactate gradient is a prerequisite for a carrier-mediated lactate flux from astrocytes to neurons

CellPress

In Vivo Evidence for a Lactate Gradient from Astrocytes to Neurons

Philipp Mächler,[1,2,6] Matthias T. Wyss,[1,2,6] Maha Elsayed,[3] Jillian Stobart,[1,2] Robin Gutierrez,[1,4]
Alexandra von Faber-Castell,[1] Vincens Kaelin,[1] Marc Zuend,[1,2] Alejandro San Martín,[4] Ignacio Romero-Gómez,[4]
Felipe Baeza-Lehnert,[4] Sylvain Lengacher,[3] Bernard L. Schneider,[3] Patrick Aebischer,[3] Pierre J. Magistretti,[3,5]
L. Felipe Barros,[4] and Bruno Weber[1,2,*]

[1]Institute of Pharmacology and Toxicology, University of Zurich, 8057 Zurich, Switzerland
[2]Neuroscience Center Zurich, University and ETH Zurich, 8092 Zurich, Switzerland
[3]Brain Mind Institute, École Polytechnique Fédérale de Lausanne, 1015 Lausanne, Switzerland
[4]Centro de Estudios Científicos, Valdivia 5110466, Chile
[5]Division of Biological and Environmental Sciences and Engineering, King Abdullah University of Science and Technology (KAUST),
Thuwal 23955-6900, Kingdom of Saudi Arabia
[6]Co-first author
*Correspondence: bweber@pharma.uzh.ch
http://dx.doi.org/10.1016/j.cmet.2015.10.010

SUMMARY

Investigating lactate dynamics in brain tissue is challenging, partly because in vivo data at cellular resolution are not available. We monitored lactate in cortical astrocytes and neurons of mice using the genetically encoded FRET sensor *Laconic* in combination with two-photon microscopy. An intravenous lactate injection rapidly increased the *Laconic* signal in both astrocytes and neurons, demonstrating high lactate permeability across tissue. The signal increase was significantly smaller in astrocytes, pointing to higher basal lactate levels in these cells, confirmed by a one-point calibration protocol. Trans-acceleration of the monocarboxylate transporter with pyruvate was able to reduce intracellular lactate in astrocytes but not in neurons. Collectively, these data provide in vivo evidence for a lactate gradient from astrocytes to neurons. This gradient is a prerequisite for a carrier-mediated lactate flux from astrocytes to neurons and thus supports the astrocyte-neuron lactate shuttle model, in which astrocyte-derived lactate acts as an energy substrate for neurons.

INTRODUCTION

The energy demand of mammalian brain tissue is met mainly by degradation of blood-borne glucose. Classical experiments with radiolabeled substrates showed label incorporation into glutamate and glutamine in a manner suggestive of two separate tricarboxylic acid cycles, a "large" and a "small" compartment (Van den Berg et al., 1969), which were assigned to neurons and astrocytes, respectively, using immunohistochemical techniques (Martinez-Hernandez et al., 1977). The concept of compartmentation in brain energy metabolism gained new momentum with the postulation of the astrocyte neuron lactate shuttle model (ANLS). In the classical version of this hypothesis,

glutamate transients are linked to a cellular compartmentation of lactate (Pellerin and Magistretti, 1994). Glutamate released from active neurons activates astrocytic glycolysis leading to production of lactate, which serves as an energy source for neurons. Increased brain lactate levels upon neuronal activation have been observed in several studies via different techniques (Hu and Wilson, 1997; Lin et al., 2010; Prichard et al., 1991; Sappey-Marinier et al., 1992). Also, L-lactate acts as a signaling molecule in certain mammalian brain regions (Mosienko et al., 2015; Tang et al., 2014; Yang et al., 2014). However, the cellular origin of lactate released during increased activity (Barros and Deitmer, 2010; Stobart and Anderson, 2013) and its significance as an energy substrate or signaling molecule remains largely unclear (Barros, 2013; Weber and Barros, 2015).

Experimental evidence from in vitro and in vivo animal studies demonstrates that lactate is able to sustain neuronal activity during glucose deprivation (Schurr, 2002; Wyss et al., 2011), and patients with non-penetrating traumatic brain injuries use peripheral lactate as brain energy substrates (for review see Glenn et al., 2015). Furthermore, lactate transport across cell membranes via monocarboxylate transporters (MCTs) is a facilitated transport (Halestrap and Wilson, 2012). Increased lactate production in one cell type and predominant lactate consumption in another cell type would therefore require a lactate concentration gradient from the "producer" to the "consumer." Lactate dehydrogenase (LDH), located in mitochondria and the surrounding cytoplasm (Brooks et al., 1999), links lactate to oxidative metabolism by catalyzing the conversion between lactate and pyruvate. The higher affinity for lactate of MCT and LDH isoforms expressed in neurons (MCT2 and LDH1) relative to the isoforms expressed in astrocytes (MCT1/4 and LDH5) supports an astrocytic production and neuronal consumption of lactate (Bittar et al., 1996; Debernardi et al., 2003; Laughton et al., 2000; Pierre and Pellerin, 2005). Inhibition of astrocytic production and neuronal consumption of lactate via LDH inhibition reduces epileptic neuronal activity, possibly due to neuronal ATP depletion (Sada et al., 2015). Moreover, the fast and transient lactate depletion in astrocytes during different in vivo and in vitro stimulation paradigms may represent the emptying of a lactate pool (Sotelo-Hitschfeld et al., 2015). Taken together, these results
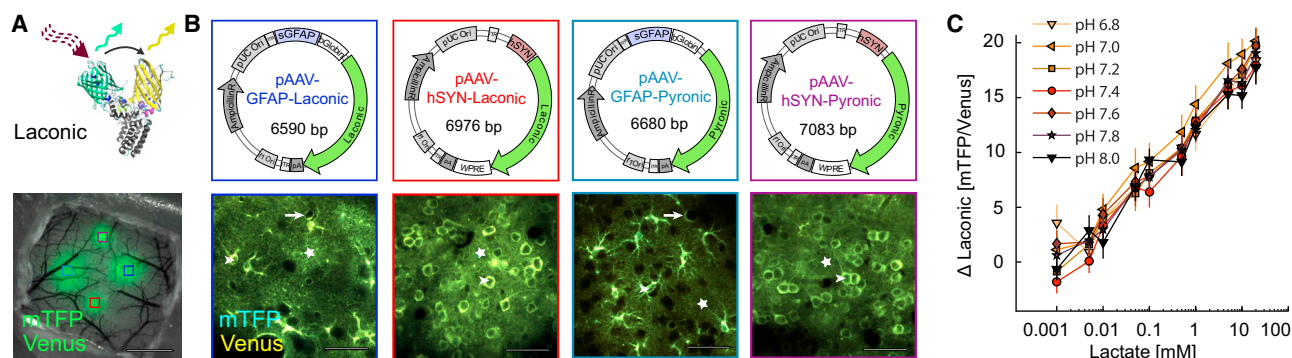
Figure 1. Expression of *Laconic* and *Pyronic* In Vivo

(A) Top: 3D structure of the lactate sensor *Laconic*, which was excited with a pulsed laser (870 nm). Emission was collected for mTFP (450–475 nm) and for Venus (535-550 nm). Botton: the fluorescence (480 nm excitation, 505–565 nm emission, green) of four individual sensors was collected through a chronic cranial window preparation of the primary somatosensory cortex of *C57BL/6* mice; scale bar, 1 mm.

(B) Top: serotype 6 adeno-associated viral vector (AAV6) with a *synapsin* promoter was used for neuronal expression, and serotype 9 vector (AAV9) with a *sGFAP* promoter for astrocytic expression. Bottom: 2PLSM at 150–250 μm below the dura shows cell-type-specific cytoplasmic sensor expression with nuclear exclusion (arrow heads), vascular endfeet (arrows), and cellular processes (stars); scale bars, 50 μm.

(C) The in vitro calibration curve of *Laconic* at 37°C shows substrate binding kinetics of lactate but no pH sensitivity. See also Figures S1A–S1E.

suggest a lactate concentration gradient from astrocytes to neurons; however, in vivo evidence of such a cellular gradient is currently absent.

Here, we investigated cell-specific lactate reservoirs in vivo employing the recently developed genetically encoded biosensor *Laconic* (San Martín et al., 2013), which we specifically expressed in astrocytes and neurons. Through two-photon laser scanning microscopy (*2PLSM*; Denk et al., 1990), we show direct indication of an in vivo lactate gradient from astrocytes to neurons.

RESULTS

Expression of *Laconic* and *Pyronic* In Vivo

To evaluate the specificity of *Laconic* transients, a biosensor construct specific for pyruvate (*Pyronic*; San Martín et al., 2014) was measured simultaneously with *Laconic*. Different adeno-associated viral (AAV) vectors, encoding either the *Laconic* or the *Pyronic* sensors, were injected in close distance to each other at the center of a craniotomy in the primary somatosensory cortex of mice (Figures 1A and S1A). The fluorescence of both sensors, driven by the short GFAP promoter, was located in the cytoplasm and showed the typical morphology of protoplasmic cortical astrocytes, including vascular endfeet and fine processes outlining dark non-fluorescent cells (Figure 1B). A similar fluorescence pattern was found throughout all imaged cortical layers, consistent with non-overlapping astrocytic domains in mice (Oberheim et al., 2009). Human synapsin promoter constructs induced cytoplasmic fluorescence in cells matching neuronal morphology, with dark nuclei and long-ranging processes toward superficial or deeper structures, located greater than 150 μm below the dura (Figure 1B). 2PLSM was restricted to layer 2/3 cells with a laser power above 20 mW to ensure stable FRET ratios (Figure S1F) and below 40 mW to prevent tissue damage and bleaching of the fluorescence. Immunohistochemical staining for GFAP, CD68, and fibrinogen revealed no increase in gliosis, microglial activity, or blood-brain barrier leakage (Figures S1A–S1D).

Laconic Sensor Functions Are Comparable In Vivo and In Vitro

L-lactate binding induces a conformational change of *Laconic*, causing a decrease in FRET efficiency, which increases the ratio of mTFP (monomeric teal fluorescent protein) over Venus (Figure 1A). In vitro lactate application leads to two-site saturable *Laconic* kinetics without pH sensitivity (Figures 1C and S1F; San Martín et al., 2013). The functionality of the sensor in vivo was demonstrated with increasing doses of sodium-L-lactate injected via a tail vein catheter during 2PLSM. *Laconic* signals in neurons and astrocytes increased non-linearly with the intravenously injected lactate dose but did not respond to 500 mM saline injections (Figures 2A and S1E). The amplitudes of *Laconic* signal changes in vivo were of the same order of magnitude as in vitro cell culture, where *Laconic* signals can be explored at a much wider range of lactate concentrations (Figure 2B).

A Single Intravenous Injection of Lactate Increases *Laconic* Signal More in Neurons Than in Astrocytes

To compare lactate accumulation in astrocytes and neurons, *Laconic* was simultaneously measured in neurons and astrocytes during short intravenous L-lactate infusions over 3 min (4 mmol/kg bodyweight), elevating blood lactate levels from 0.81 ± 0.26 mM to 17 ± 5.7 mM (Figure 3C). The *Laconic* signal increased more significantly in neurons than in astrocytes (5.7% ± 1.3% versus 4.3% ± 1.3%, respectively; Figure 3A), with a rise in extracellular lactate levels of 0.27 ± 0.08 mM (Figure 3B). This discrepancy between neurons and astrocytes could reflect higher lactate accumulation in neurons at similar baseline lactate concentrations in both cell types. Alternatively, this difference could be attributed to lower baseline lactate concentrations in neurons, which would permit a greater upward dynamic range and sensitivity of *Laconic*.

To distinguish between these two possibilities, the baseline lactate concentrations in astrocytes and neurons were compared by saturating *Laconic* in both cellular compartments.
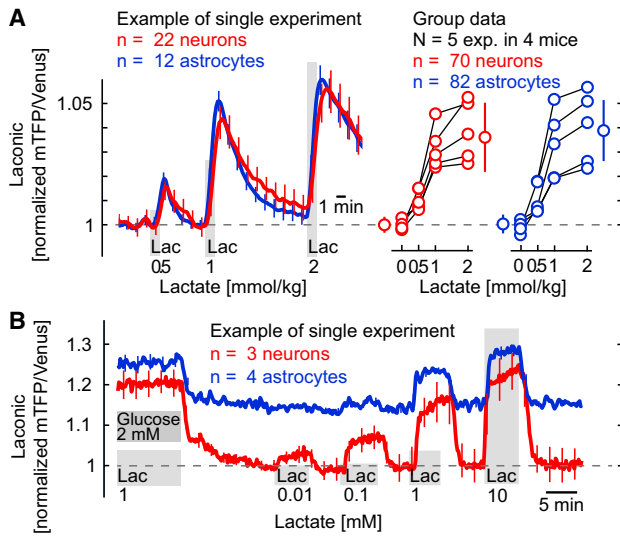
A Example of single experiment
n = 22 neurons
n = 12 astrocytes

Group data
N = 5 exp. in 4 mice
n = 70 neurons
n = 82 astrocytes

B Example of single experiment
n = 3 neurons
n = 4 astrocytes

Figure 2. *Laconic* Sensor Functions In Vivo

(A) *Laconic* signals increased in both astrocytes and neurons depending on the intravenously injected lactate dosage (Lac; 500 mM L-lactate solution; 0.5, 1, and 2 mmol/kg bodyweight; 0 mmol lactate was performed with 2 mmol/kg bodyweight of 500 mM sodium chloride solution). The SDs of cells in a single experiment (left) and of multiple independent experiments (right) are indicated (from 0 to 2 mmol/kg; normalization to individual baseline). See also Figures S1F, S1G, S3A, and S3B.

(B) Similarly, *Laconic* expressed in cultured astrocytes and neurons showed dose-dependent signal increases. Data are normalized to pyruvate-induced lactate depletion (see Figures S2D and S2E). Astrocytes, but not neurons, maintain sizable intracellular lactate levels even in a zero glucose and lactate medium, resulting in relatively low *Laconic* signal increases.

Ammonium chloride infusion over 4 min (2.5 mmol/kg bodyweight), which boosts cytosolic lactate concentration in brain cells by inhibiting mitochondrial pyruvate consumption (Lerchundi et al., 2015), increased *Laconic* signals in neurons and astrocytes ($7.3\% \pm 1.3\%$ versus $7.4\% \pm 1.6\%$, respectively; Figure S1H). When ammonium chloride and L-lactate were simultaneously infused intravenously beforehand, additional L-lactate application induced a significantly smaller increase of the *Laconic* signal in neurons ($0.95\% \pm 0.62\%$, n = 53, p < 0.05, one-sample t test) and astrocytes ($0.57\% \pm 0.55\%$, n = 43 cells, p < 0.05, one-sample t test) (Figure 4A) compared to the same lactate infusion in Figure 3 ($p < 10^{-7}$, two-sample t test). However, extracellular lactate levels continued to increase with additional lactate infusion by $16\% \pm 10.7\%$ of the total increase (p < 0.05, one-sample t test) (Figure 4B). This suggests that ammonium chloride administration increased intracellular lactate concentrations to levels that saturated *Laconic*. Overall, a greater change in neuronal *Laconic* signal was observed (ΔFRET signal: $9.9\% \pm 2.4\%$) compared to astrocytes ($6.9\% \pm 2.0\%$), supporting our hypothesis of lower baseline lactate levels in neurons (Figure 4A).

Pronounced Trans-Acceleration in Astrocytes Occurs at Baseline

Pyruvate application has been used in vitro to decrease intracellular lactate levels in erythrocytes (Fishbein et al., 1988). This effect is based on a property of MCTs called trans-acceleration
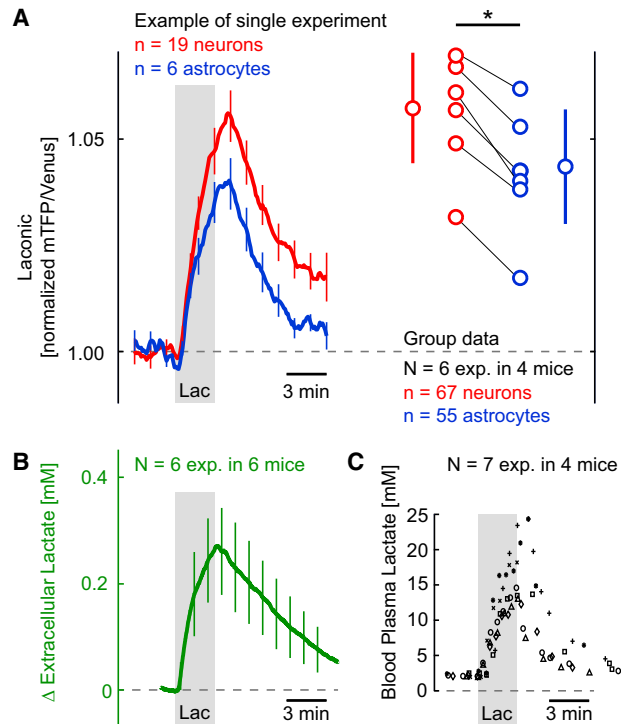
A Example of single experiment
n = 19 neurons
n = 6 astrocytes

Group data
N = 6 exp. in 4 mice
n = 67 neurons
n = 55 astrocytes

B N = 6 exp. in 6 mice

C N = 7 exp. in 4 mice

Figure 3. An Intravenous Injection of Lactate Increases *Laconic* Signals More in Neurons Than in Astrocytes

(A) Intravenous lactate infusions (4 mmol/kg bodyweight in 3 min, 500 mM solution) increased neuronal ($5.7\% \pm 1.3\%$) more than astrocytic *Laconic* signal ($4.3\% \pm 1.3\%$) in simultaneous recordings in one experiment (left) and over multiple recordings (right, normalization to individual baseline, mean on peak amplitudes, *p < 0.05). See also Figure S3C.

(B) The same lactate infusion protocol increased extracellular lactate (n = 6 animals, 0.27 ± 0.08 mM).

(C) Blood lactate concentrations rose from 0.81 ± 0.26 mM to 17 ± 5.7 mM (n = 7 experiments). Data are represented as mean ± SD.

(Figure 5E), where the presence of extracellular monocarboxylates stimulates transporter substrate efflux. This process involves a facilitated conformational switch of the substrate binding site across the cell membrane when an adequate substrate is bound (Figure S2G; Garcia et al., 1994; Halestrap, 2013).

To test the capacity of intravenously applied pyruvate to produce a trans-acceleration-induced lactate efflux out of brain cells, extracellular brain lactate levels were measured with Pinnacle biosensors (Figure S3D). Intravenous injection of 4 mmol/kg pyruvate over 3 min induced a transient increase of extracellular lactate levels of 0.084 ± 0.022 mM (Figure 5B), consistent with trans-acceleration of MCTs.

To compare trans-acceleration of MCTs in neurons and astrocytes, simultaneous measurements of *Laconic* and *Pyronic* during pyruvate application were performed. At baseline lactate levels, pyruvate decreased *Laconic* signal in astrocytes ($-4.7\% \pm 1.5\%$), while signal in neurons was relatively unchanged ($-0.6\% \pm 0.9\%$; Figure 5A). *Pyronic* showed only minor changes. However, after achieving higher intracellular lactate concentrations by the combined infusion of ammonium chloride and lactate, pyruvate administration was able to decrease *Laconic* signals in both astrocytes and neurons while increasing
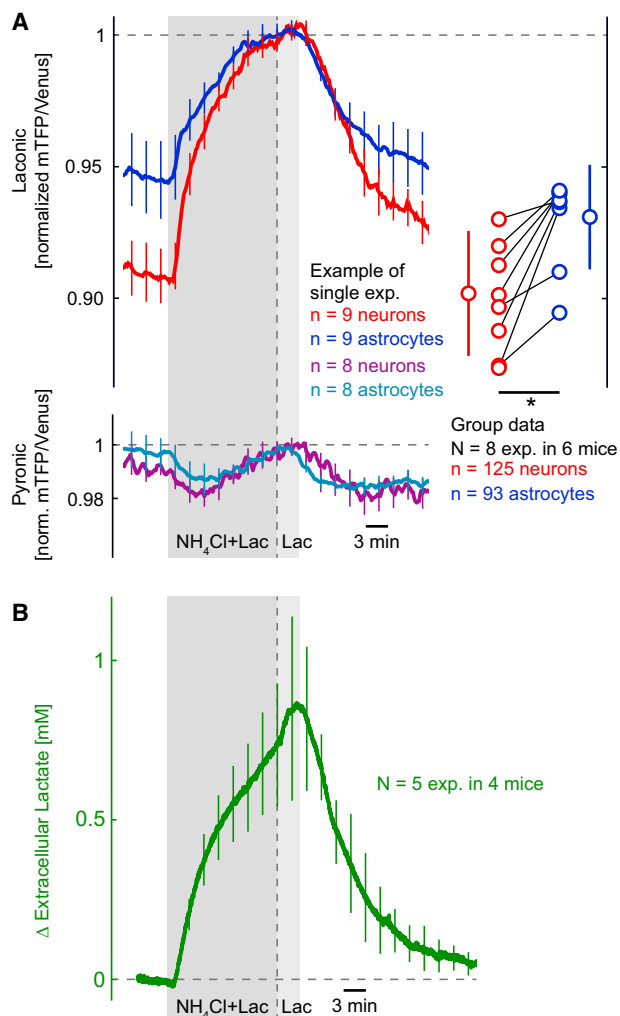
Figure 4. Baseline Lactate Levels in Astrocytes and Neurons Can Be Compared by Saturating *Laconic*

(A) Astrocytic and neuronal *Laconic* and *Pyronic* were simultaneously recorded during an intravenous infusion of ammonium chloride (4 mmol/kg bodyweight in 15 min, 500 mM solution) mixed with lactate (8 mmol/kg bodyweight in 15 min, 1 M solution), followed by a faster lactate injection (4 mmol/kg bodyweight in 3 min, 500 mM solution). *Pyronic* signals decreased during the ammonium chloride-lactate mix. In eight independent experiments, normalization to the saturation level of *Laconic* revealed lower baseline levels in neurons than in astrocytes (0.901 ± 0.024 versus 0.931 ± 0.020, normalization to the 3 min after ammonium chloride stop, mean of baseline minima, *p < 0.05).

(B) Using the same infusion protocol, changes in extracellular lactate concentrations were measured in five trials. Extracellular lactate increased until the end of the infusion protocol by 0.87 ± 0.29 mM. Data are represented as mean ± SD. See also Figures S1H and S1I.

Pyronic signals in both cells (Figure 5C). Upon repeated i.v. injections of pyruvate, neuronal *Laconic* signal kept increasing, possibly due to the conversion of pyruvate to lactate (Gonzalez et al., 2005). Under these high lactate conditions, both astrocytes and neurons show trans-acceleration (Figure 5D), demonstrating that neuronal MCTs are also susceptible to pyruvate-driven efflux (Figure 5E). In a subset of recordings, this

lactate accumulation was absent in neurons, in which case a lactate depletion during pyruvate infusions could not be observed.

DISCUSSION

The compartmentation of brain energy metabolism is a subject of intense debate, fuelled by a lack of accurate in vivo intracellular lactate measurements in different cell populations. Here, we utilized the genetically encoded lactate sensor *Laconic* to observe the capacity of blood-borne lactate to enter both astrocytes and neurons and to approximate lactate concentrations in these cells. Whole-brain tissue uptake of lactate from blood has previously been demonstrated in vivo (Cremer et al., 1979; Klein and Olsen, 1947; Wyss et al., 2011) and has been quantified in humans (Glenn et al., 2015; van Hall et al., 2009). We observed an accumulation of cellular and extracellular brain lactate during artificially increased blood lactate levels, which indicate a net uptake under these conditions and is in agreement with findings in humans (Boumezbeur et al., 2010; Quistorff et al., 2008; Rasmussen et al., 2011). The ability of neurons to take up lactate is an important prerequisite for the use of lactate as an energy substrate as suggested by the ANLS (Bélanger et al., 2011; Magistretti and Allaman, 2015), a concept that is still debated (Dienel, 2012 and references therein). Lactate has been shown to enter oxidative energy production in physiological resting conditions (Bouzier-Sore et al., 2006) and support neuronal activity under low-glucose conditions both in vitro (Tekkök et al., 2005) and in vivo (Herzog et al., 2013; Wyss et al., 2011).

We observed a greater neocortical *Laconic* signal increase in neurons than in astrocytes when blood lactate was elevated. This cell-type difference was not due to altered *Laconic* sensitivity, as cumulative signal amplitudes were similar in both populations after decreasing intracellular lactate with pyruvate infusions and normalizing to the saturated sensor (Figure S1I). Therefore, baseline neuronal lactate levels could be lower where *Laconic* is more responsive. To evaluate this possibility, *Laconic* was saturated in both cellular compartments simultaneously using a mixture of lactate and ammonium (Provent et al., 2007), which revealed a higher maximal increase of neuronal *Laconic* and suggests a lower baseline lactate concentration in neurons than in astrocytes (Figure 6A).

We utilized the trans-acceleration property of MCTs (Brown and Brooks, 1994) by applying an inward pyruvate gradient to force the cells to release their lactate. The pronounced drop of astrocytic lactate and the negligible decrease in neurons is in agreement with higher resting lactate levels in astrocytes (Figure 6B). We can reject the following alternative explanations for the astrocyte-specific lactate drop: first, cell-type-specific expression of isoforms in the brain has been reported with MCT1 mainly expressed in astrocytes and oligodendrocytes and MCT2 in neurons (Pellerin et al., 2005). We assessed the influence of MCT isoforms on trans-acceleration with a numerical model and demonstrated an almost linear dependency of the pyruvate-induced trans-acceleration on intracellular baseline lactate levels for both MCT1 and MCT2 (Figures S2A–S2C). However, the relatively higher affinity of MCT2 compared to MCT1 for pyruvate in our model would predict stronger trans-acceleration of MCT2, i.e., in neurons (Figures S2A–S2C). Also,
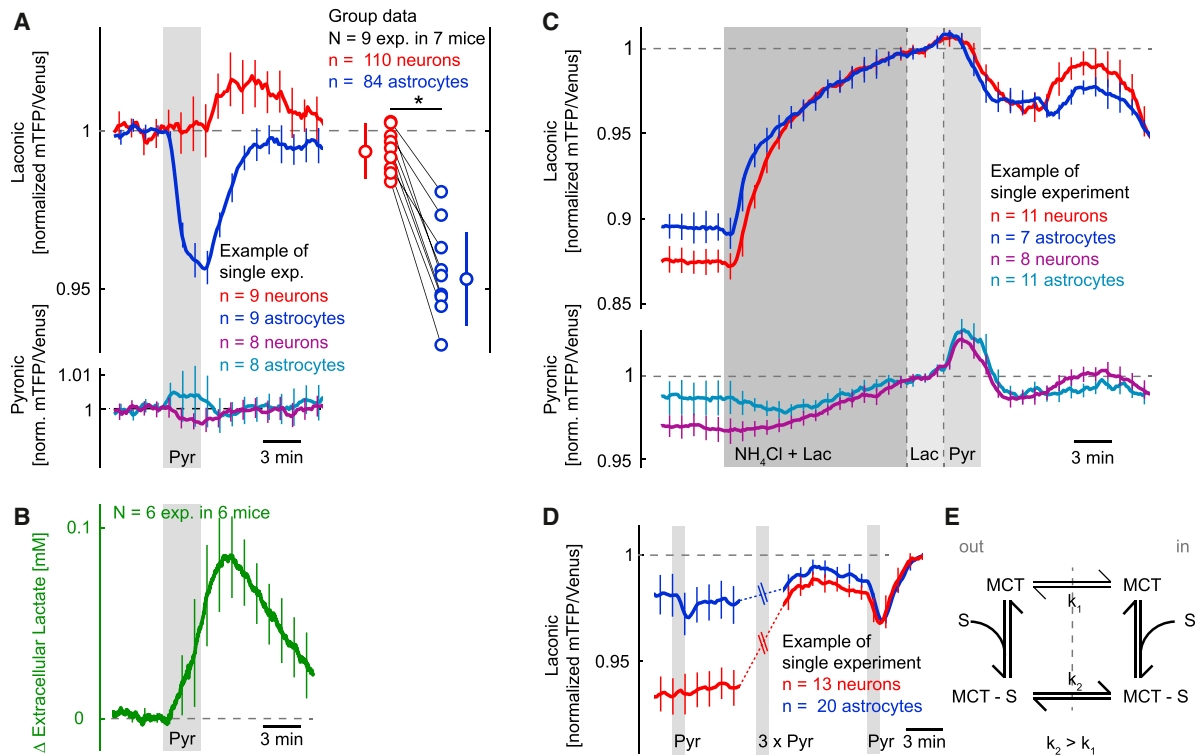
Figure 5. An Intravenous Injection of Pyruvate Decreases *Laconic* Signals More in Astrocytes Than in Neurons
(A) Intravenous pyruvate infusions (4 mmol/kg bodyweight in 3 min, 500 mM solution) decreased *Laconic* signal in astrocytes more than in neurons while inducing only minor changes in *Pyronic* signal, as observed during simultaneous recordings in one experiment (left, normalization to individual baseline). Similar effects were observed over multiple recordings (right, normalization to individual baseline, maximum decrease of astrocytes was 4.7 ± 1.5 and of neurons was 0.6 ± 0.9%; *p < 0.05).
(B) The same pyruvate infusion protocol increased extracellular lactate (n = 6 animals, 0.084 ± 0.02 mM).
(C) The *Laconic* saturation protocol (see Figure 4) was followed by a pyruvate infusion, which induced a decrease of astrocytic and neuronal *Laconic* signal and an increase in *Pyronic* signal. Normalization to 3 min after cessation of ammonium chloride infusion.
(D) In some trials repetitive pyruvate infusions increased *Laconic* signal in neurons, possibly due to conversion of pyruvate to lactate. With this artificially increased neuronal lactate levels, a pyruvate infusion (2 mmol/kg bodyweight in 1 min, 500 mM solution) induced trans-acceleration also in neurons. Normalization to last minute of trace.
(E) Trans-acceleration occurs at monocarboxylate transporters (MCT) because the substrate binding site of MCTs switches at a higher rate to the other side of the membrane when a substrate is bound (MCT – S; k_2) than without a substrate bound (MCT; k_1). Therefore, any substrate of MCT on one side of the membrane increases the rate of transport of another substrate in the opposite direction. Data are represented as mean ± SD. See also Figure S2.

trans-acceleration can be induced in cultured neurons (Figure S2E) and astrocytes (Figure S2F), where baseline lactate levels depend on the experimental conditions. The differential MCT isoform expression and kinetics can therefore not explain the predominant trans-acceleration in astrocytes.

Second, LDH diminishes lactate depletion caused by pyruvate uptake over time by transforming pyruvate into lactate. Intracellular lactate levels start to increase during pyruvate exposure if the rate of LDH-catalyzed conversion of pyruvate to lactate is high compared to lactate transport (Figure S2C), which may explain the delayed increase in lactate we observed following pyruvate infusion (Figure 5A). However, the lower NADH/NAD+ ratio in neurons compared to astrocytes (Hung et al., 2011) implies weaker conversion of pyruvate to lactate and is therefore unlikely to mask pyruvate-induced lactate depletion in neurons.

Third, the brain vasculature is almost entirely covered by astrocytic endfeet (Mathiisen et al., 2010; McCaslin et al., 2011). Therefore, astrocytes are predominantly exposed to blood-

borne pyruvate. The main transport-limiting barrier for blood-borne pyruvate to enter brain tissue is MCT1 at the endothelial membranes, and the fast diffusion within the tissue will expose all brain cells similarly (Halestrap, 2013; Miller and Oldendorf, 1986). Accordingly, we did not observe any temporal differences between astrocytic and neuronal lactate accumulation (Figures 2A and 3A). Additionally, buffering of lactate by *Laconic* is unlikely because baseline lactate levels are higher (hundreds of μM instead of nM) and lactate transients are slower (multiple seconds instead of ms) than in the case of calcium dynamics, where buffering by the sensor is reported to be an issue (Grienberger and Konnerth, 2012). Finally, increasing lactate levels in neurons lead to trans-acceleration and lactate efflux in neurons, similar to that in astrocytes (Figures 5C and 5D).

A higher resting state lactate level in astrocytes in comparison to neurons has significant implications for transcellular lactate exchange. Intracellular lactate accumulation driven by increased blood lactate and depletion during increased blood pyruvate is
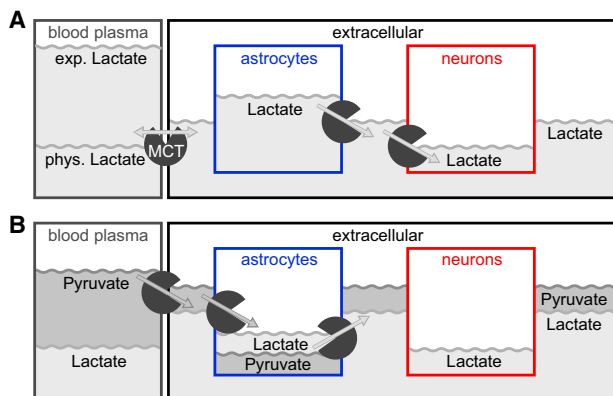
Figure 6. Model of Lactate Compartmentation

(A) Astrocytes accumulate lactate, which is transported along a concentration gradient via monocarboxylate transporters (MCT) to be consumed by neurons. Physiological (phys.) and experimentally increased (exp.) blood lactate levels are indicated.

(B) Under artificially increased blood pyruvate levels, pyruvate enters brain cells from extracellular space via MCTs, forcing the extrusion of lactate. Pyruvate entry and concurrent lactate exit via MCTs requires relatively high intracellular lactate levels.

consistent with a facilitated transport of lactate via MCTs. The direction of a facilitated transport is determined by the concentration gradient, for which we found evidence to be from astrocytes to neurons, as has been suggested by the ANLS (Pellerin and Magistretti, 1994) (Figure 6A). However, alternative lactate transport mechanisms have been suggested, such as via pannexins and connexins (Barros, 2013; Giaume et al., 2013) or an unknown potassium-dependent ion channel, which would allow active lactate transport even against a chemical concentration gradient during increased neuronal activity (Sotelo-Hitschfeld et al., 2015).

In addition, astrocytic lactate could provide a small but fast energy reserve; cultured astrocytes have been shown to preferentially export glucose-derived lactate rather than lactate derived from glycogen (Sickmann et al., 2005). Glycogen may serve as a slower energy pool, as astrocytic glycogen-derived lactate sustains neuronal function in rat optical nerve preparations for several minutes (Brown and Ransom, 2007).

Our data provide important information about lactate concentrations of the different cellular compartments, which are fundamental for the role of lactate as an activity-dependent signaling molecule (Mosienko et al., 2015). The transport of lactate from astrocytes to neurons has been shown to be necessary for the establishment of long-term memory (Suzuki et al., 2011) by inducing the expression of plasticity-related genes (Yang et al., 2014). Volatile halogenated anesthetics such as isoflurane are known to increase brain lactate levels (Boretius et al., 2013; Horn and Klein, 2010), and Fünfschilling et al. (2012) reported a marked decrease in tissue lactate concentration in response to the discontinuation of isoflurane anesthesia, indicative of a substantial lactate exchange. In our study, we used injectable anesthetics to avoid elevated lactate levels, but our results can be used to interpret the direction of isoflurane-induced lactate exchange at the cellular level. It is important to note, however, that *Laconic* did not enable us to measure cellular or whole-brain

lactate transport or oxidation rates in vivo, as currently available pharmacological agents (such as the MCT blocker α-cyano-4-hydroxycinnamate) are neither fast (seconds) nor specific (limited side effects) enough.

In summary, the genetically encoded lactate sensor *Laconic* in combination with 2PLSM was successfully applied to investigate brain energy metabolism at the single-cell level in vivo. We demonstrate that neurons and astrocytes readily take up blood-borne lactate. Our data suggest a significantly lower baseline lactate level in neurons in comparison to astrocytes. Our findings furthermore support the concept of compartmentalized lactate pools with a lactate flux from astrocytes to neurons.

EXPERIMENTAL PROCEDURES

Viral Constructs of the Lactate Sensor *Laconic* and the Pyruvate Sensor *Pyronic*

Genetically encoded FRET sensors for lactate (*Laconic*; San Martín et al., 2013) and pyruvate (*Pyronic*; San Martín et al., 2014) were cloned into AAV plasmids for astrocyte- and neuron-specific expression. The astrocyte-specific construct included a minimal GFAP promoter (GfaABC$_1$D, sGFAP; kindly provided by Dr. M. Brenner, Department of Neurobiology, University of Alabama) (Lee et al., 2008), a beta-globin intron, and a poly-adenylation signal. The neuronal construct included a human synapsin-1 (SYN) promoter, a woodchuck hepatitis virus (WHP) post-transcriptional regulatory element (WPRE), and a poly-adenylation signal (Glover et al., 2002; Kügler et al., 2001). The four different shuttle plasmids (pAAV-SYN-*Laconic*, pAAV-GFAP-*Laconic*, pAAV-SYN-*Pyronic*, and pAAV-GFAP-*Pyronic*) were used to generate AAV serotype 6 (SYN constructs) or AAV serotype 9 (GFAP constructs) viral particles by co-transfecting the shuttle plasmid with the pDP6 and pDF9 helper plasmids in HEK293-AAV cells (Agilent Technologies). Viral particles were isolated from the cell lysates using iodixanol step gradients and HPLC purification on heparin-binding (AAV6) and ion exchange (AAV9) columns. The number of viral genomic copies (VG) was measured by TaqMan real-time PCR, with primers amplifying specific sequences in the human beta-globin intron or WPRE element.

Animals

All experimental procedures were approved by the local veterinary authorities in Zurich and conformed to the guidelines of the Swiss Animal Protection Law, Veterinary Office, Canton of Zurich (Act of Animal Protection 16 December 2005 and Animal Protection Ordinance 23 April 2008). Surgery was performed in female wild-type mice (*C57BL/6J*; Charles River) of 8–10 weeks of age (20–25 g bodyweight). The mice had free access to water and food and an inverted 12 hr light/dark cycle.

Anesthesia

The animals were anesthetized with a mixture of fentanyl (0.05 mg/kg bodyweight; Sintenyl, Sintetica), midazolam (5 mg/kg bodyweight; Dormicum, Roche), and medetomidine (0.5 mg/kg bodyweight; Domitor, Orion Pharma) intraperitoneally, and anesthesia was maintained with midazolam (5 mg/kg bodyweight) subcutaneously after 50 min. To prevent hypoxemia, a face mask provided 300 ml/min of 100% oxygen. Core temperature was kept constant at 37°C using a homeothermic blanket heating system during all surgical and experimental procedures (Harvard Apparatus). The head was fixed in a stereotaxic apparatus and the eyes were kept wet with ointment (vitamin A eye cream; Bausch & Lomb).

Virus Injection

A 4 × 4 mm craniotomy was performed above the somatosensory cortex using a dental drill (Bien-Air), and solutions containing virus vector were injected into the primary somatosensory cortex at a close distance to achieve neighboring, but non-overlapping, sensor protein expression: 75 nl of AAV9-GFAP-*Laconic* (titer 3.1 E12 VG/ml); 150 nl of AAV6-SYN-*Laconic* (titer 1.02 E13 VG/ml) (San Martín et al., 2013); 75 nl of AAV9-GFAP-*Pyronic* (titer 1.6 E12 VG/ml); 150 nl of AAV6-SYN-*Pyronic* (titer 1.15 E12 VG/ml) (San Martín et al., 2014). Large

vessels were avoided to prevent bleeding and the absorption of light by hemoglobin during imaging. A square coverslip (3 × 3 mm, UQG Optics) was placed on the exposed dura mater and fixed to the skull with dental cement, according to published protocols (Holtmaat et al., 2009).

Head-Post Implantation
A bonding agent (Gluma Comfort Bond; Heraeus Kulzer) was applied to the cleaned skull and polymerized with a handheld blue light source (600 mW/cm^2; Demetron LC). A custom-made aluminum head post was connected with dental cement (EvoFlow; Ivoclar Vivadent AG) to the bonding agent for later reproducible animal fixation in the microscope setup. The skin lesion was treated with antibiotic ointment (Neomycin, Cicatrex; Janssen-Cilag AG) and closed with acrylic glue (Histoacryl, B. Braun). After surgery the animals were kept warm and provided with analgesics (metamizole 0.2 mg/g bodyweight; Sintetica), and an antibiotic was added to the drinking water (enrofloxacin, 200 mg/l drinking water; Baytril, Bayer). Sensor protein expression was checked using a fluorescence stereomicroscope (Leica MZ16 FA) 2–3 weeks after virus injection and prior to imaging.

Intracellular Lactate Measurements
The mice were imaged using a custom-built two-photon laser scanning microscope (2PLSM) (Mayrhofer et al., 2015) with a tunable pulsed laser (MaiTai eHP DS system, Spectra-Physics) at 870 nm wavelength and equipped with a 20× water immersion objective (W-Plan-Apochromat 20×/1.0 differential interference contrast, Zeiss). During measurements, the animals were head-fixed and kept under the anesthesia described above. The galvo-mirrors and a motorized objective were used to cycle through 2–4 individual fields of view. Unidirectional frame scans at 0.1 Hz and 512 × 512 pixel resolution were acquired with ScanImage (r3.8.1; Janelia Research Campus; Pologruto et al., 2003). Lactate concentration in cultured cells was measured with the use of *Laconic* as previously described (Sotelo-Hitschfeld et al., 2015).

Extracellular Lactate Measurements
Extracellular lactate measurements were performed with a commercially available recording system (Pinnacle Technology). Mice were fixed in a stereotactic frame under anesthesia (isoflurane 1.5%; Abbott), the skull was opened with a dental drill, and a guide cannula (Part 7032, Pinnacle Technology) was implanted into the primary somatosensory cortex (from bregma: A/P +1.41, M/L −2.8, D/V −1.0) and fixed with dental cement to an anchor screw (Part 8209, Pinnacle Technology). After a recovery period of 2 weeks, the pre-calibrated lactate biosensor was inserted into the guide cannula (Naylor et al., 2012). A tail vein catheter was inserted for saline, lactate, and pyruvate infusions. Recording started after 1 hr of signal stabilization.

Blood Lactate Level Measurements
The femoral artery was exposed and cannulated with fine bore polyethylene tubing (0.28 mm ID, 0.61 mm OD, Portex, Smith Medical) to measure blood lactate level. Blood drops were removed from the cannula and every fourth drop was used for an enzymatic lactate assay (Lactate Pro 2, Arkray). After each blood sample analysis, the tubing was rinsed with heparinized (50 IU/ml) 0.9% saline solution.

Intervention Protocols
For intravenous interventions, a 30G needle was connected to fine bore polyethylene tubing (0.28 mm ID, 0.61 mm OD, Portex, Smith Medical), filled with 0.9% saline solution, and inserted into one of the tail veins. Before imaging, the tubing was connected via an X connector (model *SC25*, Instech) to peristaltic pumps (Reglo digital ISM 831, Ismatec SA), which were operated via custom written Matlab codes. A 500 mM solution of sodium chloride (*S7653*, Sigma-Aldrich), sodium L-lactate (*L7022*, Sigma-Aldrich), or sodium pyruvate (*P2256*, Sigma-Aldrich) at 4 mmol/kg bodyweight was injected during 3 min.

Immunohistochemistry
Four mice expressing astrocytic and neuronal *Laconic* sensors and one mouse intraperitoneally injected with 2 mg/kg bodyweight lipopolysaccharides (Fontana et al., 1981) were anesthetized with pentobarbital (Nembutal, >50 mg/kg) intraperitoneally and transcardially perfused with 2% paraformaldehyde to assess immunohistochemical alterations. Brains were post-fixed in 4% paraformaldehyde, rinsed with phosphate-buffered saline (PBS), and cryoprotected with 30% sucrose in PBS. The frozen brains were then cut into 40 μm sections with a sliding microtome, and fluorescent regions were identified with a fluorescence stereomicroscope (Leica MZ16 FA; Leica Microsystems). Free-floating sections were incubated with rabbit anti-Glial fibrillary acidic protein (GFAP) antibody (*Z0334*; DakoCytomation), rabbit anti-fibrinogen antibody (*A0080*; DakoCytomation), or rat anti-CD68 antibody (*MCA1957GA*; AbD Serotec) and stained with red fluorescent secondary antibody (goat anti-rabbit and goat anti-rat Cy3; Jackson ImmunoResearch Laboratories). Images of the sections were collected with a laser-scanning confocal microscope (LSM510-Meta; Zeiss).

Cell Culture Experiments
All animal procedures for the cell culture experiments were approved by the Institutional Animal Care and Use Committee of the Centro de Estudios Científicos. Mixed cortical cultures of neuronal and glial cells were prepared from 1- to 3-day-old neonates (*C57BL/6J*) as detailed previously (Bittner et al., 2010). For *Laconic* sensor expression, cultures were exposed to 5 × 10^6 PFU of *Ad Laconic* and studied after 48 hr (culture day 8–10). The co-culture cells were imaged with an upright Olympus FV1000 confocal microscope and a 440 nm solid-state laser as detailed previously (Sotelo-Hitschfeld et al., 2015). Masked ratio images were generated from background-subtracted images using ImageJ software.

Data Analysis and Statistics
Astrocytic domains and neuronal cytoplasm of individual cells of cortical layers L2/3 (150–250 μm below the dura) were outlined using ImageJ (1.46r; NIH). The mTFP channel (with bandpass filter 475/64; Semrock) was divided by the Venus channel (with bandpass filter 542/50; Semrock), and the ratio was normalized to the corresponding baseline or as indicated in the figure legend using Matlab (MathWorks). Time acquisition curves are filtered with a moving average of five frames and indicated as mean ± SD. Effects in multiple animals were compared using t tests in R (R Core Team, 2014). p values < 0.05 were taken as the significance limit.

SUPPLEMENTAL INFORMATION

Supplemental Information includes three figures and can be found with this article online at http://dx.doi.org/10.1016/j.cmet.2015.10.010.

REFERENCES

Barros, L.F. (2013). Metabolic signaling by lactate in the brain. Trends Neurosci. *36*, 396–404.

Barros, L.F., and Deitmer, J.W. (2010). Glucose and lactate supply to the synapse. Brain Res. Brain Res. Rev. *63*, 149–159.

Bélanger, M., Allaman, I., and Magistretti, P.J. (2011). Brain energy metabolism: focus on astrocyte-neuron metabolic cooperation. Cell Metab. *14*, 724–738.

Bittar, P.G., Charnay, Y., Pellerin, L., Bouras, C., and Magistretti, P.J. (1996). Selective distribution of lactate dehydrogenase isoenzymes in neurons and astrocytes of human brain. J. Cereb. Blood Flow Metab. *16*, 1079–1089.

Bittner, C.X., Loaiza, A., Ruminot, I., Larenas, V., Sotelo-Hitschfeld, T., Gutiérrez, R., Córdova, A., Valdebenito, R., Frommer, W.B., and Barros, L.F. (2010). High resolution measurement of the glycolytic rate. Front. Neuroenergetics *2*, 2.

Boretius, S., Tammer, R., Michaelis, T., Brockmöller, J., and Frahm, J. (2013). Halogenated volatile anesthetics alter brain metabolism as revealed by proton magnetic resonance spectroscopy of mice in vivo. Neuroimage *69*, 244–255.

Boumezbeur, F., Petersen, K.F., Cline, G.W., Mason, G.F., Behar, K.L., Shulman, G.I., and Rothman, D.L. (2010). The contribution of blood lactate to brain energy metabolism in humans measured by dynamic 13C nuclear magnetic resonance spectroscopy. J. Neurosci. *30*, 13983–13991.

Bouzier-Sore, A.-K., Voisin, P., Bouchaud, V., Bezancon, E., Franconi, J.-M., and Pellerin, L. (2006). Competition between glucose and lactate as oxidative energy substrates in both neurons and astrocytes: a comparative NMR study. Eur. J. Neurosci. *24*, 1687–1694.

Brooks, G.A., Dubouchaud, H., Brown, M., Sicurello, J.P., and Butz, C.E. (1999). Role of mitochondrial lactate dehydrogenase and lactate oxidation in the intracellular lactate shuttle. Proc. Natl. Acad. Sci. USA *96*, 1129–1134.

Brown, M.A., and Brooks, G.A. (1994). Trans-stimulation of lactate transport from rat sarcolemmal membrane vesicles. Arch. Biochem. Biophys. *313*, 22–28.

Brown, A.M., and Ransom, B.R. (2007). Astrocyte glycogen and brain energy metabolism. Glia *55*, 1263–1271.

Cremer, J.E., Cunningham, V.J., Pardridge, W.M., Braun, L.D., and Oldendorf, W.H. (1979). Kinetics of blood-brain barrier transport of pyruvate, lactate and glucose in suckling, weanling and adult rats. J. Neurochem. *33*, 439–445.

Debernardi, R., Pierre, K., Lengacher, S., Magistretti, P.J., and Pellerin, L. (2003). Cell-specific expression pattern of monocarboxylate transporters in astrocytes and neurons observed in different mouse brain cortical cell cultures. J. Neurosci. Res. *73*, 141–155.

Denk, W., Strickler, J.H., and Webb, W.W. (1990). Two-photon laser scanning fluorescence microscopy. Science *248*, 73–76.

Dienel, G.A. (2012). Brain lactate metabolism: the discoveries and the controversies. J. Cereb. Blood Flow Metab. *32*, 1107–1138.

Fishbein, W.N., Foellmer, J.W., Davis, J.I., Fishbein, T.M., and Armbrustmacher, P. (1988). Clinical assay of the human erythrocyte lactate transporter. I. Principles, procedure, and validation. Biochem. Med. Metab. Biol. *39*, 338–350.

Fontana, A., Bosshard, R., Dahinden, C., Grob, P., and Grieder, A. (1981). Glia cell response to bacterial lipopolysaccharide: effect on nucleotide synthesis, its genetic control and definition of the active principle. J. Neuroimmunol. *1*, 343–352.

Fünfschilling, U., Supplie, L.M., Mahad, D., Boretius, S., Saab, A.S., Edgar, J., Brinkmann, B.G., Kassmann, C.M., Tzvetanova, I.D., Möbius, W., et al. (2012). Glycolytic oligodendrocytes maintain myelin and long-term axonal integrity. Nature *485*, 517–521.

Garcia, C.K., Goldstein, J.L., Pathak, R.K., Anderson, R.G.W., and Brown, M.S. (1994). Molecular characterization of a membrane transporter for lactate, pyruvate, and other monocarboxylates: implications for the Cori cycle. Cell *76*, 865–873.

Giaume, C., Leybaert, L., Naus, C.C., and Sáez, J.C. (2013). Connexin and pannexin hemichannels in brain glial cells: properties, pharmacology, and roles. Front. Pharmacol. *4*, 88.

Glenn, T.C., Martin, N.A., Horning, M.A., McArthur, D.L., Hovda, D.A., Vespa, P., and Brooks, G.A. (2015). Lactate: brain fuel in human traumatic brain injury: a comparison with normal healthy control subjects. J. Neurotrauma *32*, 820–832.

Glover, C.P.J., Bienemann, A.S., Heywood, D.J., Cosgrave, A.S., and Uney, J.B. (2002). Adenoviral-mediated, high-level, cell-specific transgene expression: a SYN1-WPRE cassette mediates increased transgene expression with no loss of neuron specificity. Mol. Ther. *5*, 509–516.

Gonzalez, S.V., Nguyen, N.H.T., Rise, F., and Hassel, B. (2005). Brain metabolism of exogenous pyruvate. J. Neurochem. *95*, 284–293.

Grienberger, C., and Konnerth, A. (2012). Imaging calcium in neurons. Neuron *73*, 862–885.

Halestrap, A.P. (2013). Monocarboxylic acid transport. Compr. Physiol. *3*, 1611–1643.

Halestrap, A.P., and Wilson, M.C. (2012). The monocarboxylate transporter family–role and regulation. IUBMB Life *64*, 109–119.

Herzog, R.I., Jiang, L., Herman, P., Zhao, C., Sanganahalli, B.G., Mason, G.F., Hyder, F., Rothman, D.L., Sherwin, R.S., and Behar, K.L. (2013). Lactate preserves neuronal metabolism and function following antecedent recurrent hypoglycemia. J. Clin. Invest. *123*, 1988–1998.

Holtmaat, A., Bonhoeffer, T., Chow, D.K., Chuckowree, J., De Paola, V., Hofer, S.B., Hübener, M., Keck, T., Knott, G., Lee, W.-C.A., et al. (2009). Long-term, high-resolution imaging in the mouse neocortex through a chronic cranial window. Nat. Protoc. *4*, 1128–1144.

Horn, T., and Klein, J. (2010). Lactate levels in the brain are elevated upon exposure to volatile anesthetics: a microdialysis study. Neurochem. Int. *57*, 940–947.

Hu, Y., and Wilson, G.S. (1997). A temporary local energy pool coupled to neuronal activity: fluctuations of extracellular lactate levels in rat brain monitored with rapid-response enzyme-based sensor. J. Neurochem. *69*, 1484–1490.

Hung, Y.P., Albeck, J.G., Tantama, M., and Yellen, G. (2011). Imaging cytosolic NADH-NAD(+) redox state with a genetically encoded fluorescent biosensor. Cell Metab. *14*, 545–554.

Klein, J.R., and Olsen, N.S. (1947). Distribution of intravenously injected glutamate, lactate, pyruvate, and succinate between blood and brain. J. Biol. Chem. *167*, 1–5.

Kügler, S., Meyn, L., Holzmüller, H., Gerhardt, E., Isenmann, S., Schulz, J.B., and Bähr, M. (2001). Neuron-specific expression of therapeutic proteins: evaluation of different cellular promoters in recombinant adenoviral vectors. Mol. Cell. Neurosci. *17*, 78–96.

Laughton, J.D., Charnay, Y., Belloir, B., Pellerin, L., Magistretti, P.J., and Bouras, C. (2000). Differential messenger RNA distribution of lactate dehydrogenase LDH-1 and LDH-5 isoforms in the rat brain. Neuroscience *96*, 619–625.

Lee, Y., Messing, A., Su, M., and Brenner, M. (2008). GFAP promoter elements required for region-specific and astrocyte-specific expression. Glia *56*, 481–493.

Lerchundi, R., Fernández-Moncada, I., Contreras-Baeza, Y., Sotelo-Hitschfeld, T., Mächler, P., Wyss, M.T., Stobart, J., Baeza-Lehnert, F., Alegría, K., Weber, B., and Barros, L.F. (2015). NH4+ triggers the release of astrocytic lactate via mitochondrial pyruvate shunting. Proc. Natl. Acad. Sci. USA *112*, 11090–11095.

Lin, A.-L., Fox, P.T., Hardies, J., Duong, T.Q., and Gao, J.-H. (2010). Nonlinear coupling between cerebral blood flow, oxygen consumption, and ATP production in human visual cortex. Proc. Natl. Acad. Sci. USA *107*, 8446–8451.

Magistretti, P.J., and Allaman, I. (2015). A cellular perspective on brain energy metabolism and functional imaging. Neuron *86*, 883–901.

Martinez-Hernandez, A., Bell, K.P., and Norenberg, M.D. (1977). Glutamine synthetase: glial localization in brain. Science *195*, 1356–1358.

Mathiisen, T.M., Lehre, K.P., Danbolt, N.C., and Ottersen, O.P. (2010). The perivascular astroglial sheath provides a complete covering of the brain microvessels: an electron microscopic 3D reconstruction. Glia *58*, 1094–1103.

Mayrhofer, J., Haiss, F., Haenni, D., Weber, S., Zuend, M., Barrett, M., Ferrari, K., Maechler, P., Saab, A., Stobart, J., et al. (2015). Design and performance of an ultra-flexible two-photon microscope for in vivo research. Biomed. Opt. Express *6*, 4228–4237.

McCaslin, A.F.H., Chen, B.R., Radosevich, A.J., Cauli, B., and Hillman, E.M.C. (2011). In vivo 3D morphology of astrocyte-vasculature interactions in the somatosensory cortex: implications for neurovascular coupling. J. Cereb. Blood Flow Metab. *31*, 795–806.

Miller, L.P., and Oldendorf, W.H. (1986). Regional kinetic constants for blood-brain barrier pyruvic acid transport in conscious rats by the monocarboxylic acid carrier. J. Neurochem. *46*, 1412–1416.

Mosienko, V., Teschemacher, A.G., and Kasparov, S. (2015). Is L-lactate a novel signaling molecule in the brain? J. Cereb. Blood Flow Metab. *35*, 1069–1075.

Naylor, E., Aillon, D.V., Barrett, B.S., Wilson, G.S., Johnson, D.A., Johnson, D.A., Harmon, H.P., Gabbert, S., and Petillo, P.A. (2012). Lactate as a biomarker for sleep. Sleep *35*, 1209–1222.

Oberheim, N.A., Takano, T., Han, X., He, W., Lin, J.H.C., Wang, F., Xu, Q., Wyatt, J.D., Pilcher, W., Ojemann, J.G., et al. (2009). Uniquely hominid features of adult human astrocytes. J. Neurosci. *29*, 3276–3287.

Pellerin, L., and Magistretti, P.J. (1994). Glutamate uptake into astrocytes stimulates aerobic glycolysis: a mechanism coupling neuronal activity to glucose utilization. Proc. Natl. Acad. Sci. USA *91*, 10625–10629.

Pellerin, L., Bergersen, L.H., Halestrap, A.P., and Pierre, K. (2005). Cellular and subcellular distribution of monocarboxylate transporters in cultured brain cells and in the adult brain. J. Neurosci. Res. *79*, 55–64.

Pierre, K., and Pellerin, L. (2005). Monocarboxylate transporters in the central nervous system: distribution, regulation and function. J. Neurochem. *94*, 1–14.

Pologruto, T.A., Sabatini, B.L., and Svoboda, K. (2003). ScanImage: flexible software for operating laser scanning microscopes. Biomed. Eng. Online *2*, 13.

Prichard, J., Rothman, D., Novotny, E., Petroff, O., Kuwabara, T., Avison, M., Howseman, A., Hanstock, C., and Shulman, R. (1991). Lactate rise detected by 1H NMR in human visual cortex during physiologic stimulation. Proc. Natl. Acad. Sci. USA *88*, 5829–5831.

Provent, P., Kickler, N., Barbier, E.L., Bergerot, A., Farion, R., Goury, S., Marcaggi, P., Segebarth, C., and Coles, J.A. (2007). The ammonium-induced increase in rat brain lactate concentration is rapid and reversible and is compatible with trafficking and signaling roles for ammonium. J. Cereb. Blood Flow Metab. *27*, 1830–1840.

Quistorff, B., Secher, N.H., and Van Lieshout, J.J. (2008). Lactate fuels the human brain during exercise. FASEB J. *22*, 3443–3449.

R Core Team (2014). R: A Language and Environment for Statistical Computing (Vienna, Austria: R Foundation for Statistical Computing).

Rasmussen, P., Wyss, M.T., and Lundby, C. (2011). Cerebral glucose and lactate consumption during cerebral activation by physical activity in humans. FASEB J. *25*, 2865–2873.

Sada, N., Lee, S., Katsu, T., Otsuki, T., and Inoue, T. (2015). Epilepsy treatment. Targeting LDH enzymes with a stiripentol analog to treat epilepsy. Science *347*, 1362–1367.

San Martín, A., Ceballo, S., Ruminot, I., Lerchundi, R., Frommer, W.B., and Barros, L.F. (2013). A genetically encoded FRET lactate sensor and its use to detect the Warburg effect in single cancer cells. PLoS ONE *8*, e57712.

San Martín, A., Ceballo, S., Baeza-Lehnert, F., Lerchundi, R., Valdebenito, R., Contreras-Baeza, Y., Alegría, K., and Barros, L.F. (2014). Imaging mitochondrial flux in single cells with a FRET sensor for pyruvate. PLoS ONE *9*, e85780.

Sappey-Marinier, D., Calabrese, G., Fein, G., Hugg, J.W., Biggins, C., and Weiner, M.W. (1992). Effect of photic stimulation on human visual cortex lactate and phosphates using 1H and 31P magnetic resonance spectroscopy. J. Cereb. Blood Flow Metab. *12*, 584–592.

Schurr, A. (2002). Lactate, glucose and energy metabolism in the ischemic brain (Review). Int. J. Mol. Med. *10*, 131–136.

Sickmann, H.M., Schousboe, A., Fosgerau, K., and Waagepetersen, H.S. (2005). Compartmentation of lactate originating from glycogen and glucose in cultured astrocytes. Neurochem. Res. *30*, 1295–1304.

Sotelo-Hitschfeld, T., Niemeyer, M.I., Mächler, P., Ruminot, I., Lerchundi, R., Wyss, M.T., Stobart, J., Fernández-Moncada, I., Valdebenito, R., Garrido-Gerter, P., et al. (2015). Channel-mediated lactate release by K$^+$-stimulated astrocytes. J. Neurosci. *35*, 4168–4178.

Stobart, J.L., and Anderson, C.M. (2013). Multifunctional role of astrocytes as gatekeepers of neuronal energy supply. Front. Cell. Neurosci. *7*, 38.

Suzuki, A., Stern, S.A., Bozdagi, O., Huntley, G.W., Walker, R.H., Magistretti, P.J., and Alberini, C.M. (2011). Astrocyte-neuron lactate transport is required for long-term memory formation. Cell *144*, 810–823.

Tang, F., Lane, S., Korsak, A., Paton, J.F.R., Gourine, A.V., Kasparov, S., and Teschemacher, A.G. (2014). Lactate-mediated glia-neuronal signalling in the mammalian brain. Nat. Commun. *5*, 3284.

Tekkök, S.B., Brown, A.M., Westenbroek, R., Pellerin, L., and Ransom, B.R. (2005). Transfer of glycogen-derived lactate from astrocytes to axons via specific monocarboxylate transporters supports mouse optic nerve activity. J. Neurosci. Res. *81*, 644–652.

Van den Berg, C.J., Krzalić, L., Mela, P., and Waelsch, H. (1969). Compartmentation of glutamate metabolism in brain. Evidence for the existence of two different tricarboxylic acid cycles in brain. Biochem. J. *113*, 281–290.

van Hall, G., Strømstad, M., Rasmussen, P., Jans, O., Zaar, M., Gam, C., Quistorff, B., Secher, N.H., and Nielsen, H.B. (2009). Blood lactate is an important energy source for the human brain. J. Cereb. Blood Flow Metab. *29*, 1121–1129.

Weber, B., and Barros, L.F. (2015). The Astrocyte: Powerhouse and Recycling Center. Cold Spring Harb. Perspect. Biol. a020396, http://dx.doi.org/10.1101/cshperspect.a020396.

Wyss, M.T., Jolivet, R., Buck, A., Magistretti, P.J., and Weber, B. (2011). In vivo evidence for lactate as a neuronal energy source. J. Neurosci. *31*, 7477–7485.

Yang, J., Ruchti, E., Petit, J.-M., Jourdain, P., Grenningloh, G., Allaman, I., and Magistretti, P.J. (2014). Lactate promotes plasticity gene expression by potentiating NMDA signaling in neurons. Proc. Natl. Acad. Sci. USA *111*, 12228–12233.